Agricultural and Forest Meteorology 181 (2013) 17–32

Contents lists available at ScienceDirect

Agricultural and Forest Meteorology

journal homepage: www.elsevier.com/locate/agrformet

Eddy covariance measurements with a new fast-response, enclosed-path analyzer: Spectral characteristics and cross-system comparisons

K.A. Novick[a,d,*], J. Walker[b], W.S. Chan[c], A. Schmidt[c], C. Sobek[a], J.M. Vose[a]

[a] USDA Forest Service, Coweeta Hydrologic Laboratory, 3160 Coweeta Lab Road, Otto, NC 28734, United States
[b] US EPA National Risk Management Research Laboratory, 109 T.W. Alexander Dr. Mail Drop E305-02. RTP, Durham, NC 2771, United States
[c] Department of Forest Ecosystems and Society, Oregon State University, Corvallis, OR 97331, United States
[d] School of Public and Environmental Affairs, Indiana University, 702 N. Walnut Grove Avenue, Bloomington, IN, 47405, United States

ARTICLE INFO

Article history:
Received 17 September 2012
Received in revised form 21 June 2013
Accepted 24 June 2013

Keywords:
Eddy covariance
Spectra
Density corrections
Instrument heating
Closed-path
Open-path

ABSTRACT

A new class of enclosed path gas analyzers suitable for eddy covariance applications combines the advantages of traditional closed-path systems (small density corrections, good performance in poor weather) and open-path systems (good spectral response, low power requirements), and permits estimates of instantaneous gas mixing ratio. Here, the extent to which these advantages are realized in field deployment is assessed, with a focus on the suitability of such an analyzer (the EC155, manufactured by Campbell Scientific) for long-term flux measurements in a new flux monitoring site in the southern Appalachians (NC, USA). The scalar-vertical velocity co-spectra for CO_2 fluxes measured with the EC155 were similar to those measured with a co-located open-path system. When humidity was high, attenuation of the EC155 water vapor fluxes for non-dimensional frequencies greater than ~2 was noted, though results from an ogive analysis suggest that eddies operating on these time scales contributed <2% of the total turbulent flux in this tall forest ecosystem. Inertial sub-range decay of the vertical velocity-scalar co-spectra generally conformed to a -7/3 power law during near-neutral atmospheric stability conditions, supporting the use of an analytical spectral correction approach to the raw measured fluxes. The EC155 fluxes computed directly from instantaneous mixing ratio agreed with will those calculated from mass–density concentration measurements, provided density terms for temperature, water vapor, and pressure were applied. Biases were observed when the EC155 flux records were compared to those measured with the open-path system. These differences were related to wind angle of attack and to an estimate of apparent fluxes related to instrument self-heating, and the biases were minimized after the application of a friction velocity filter. Finally, the EC155 considerably outperformed open-path analyzers during adverse weather conditions favorable to fog development, which occur frequently in the study site.

Published by Elsevier B.V.

1. Introduction

Within the FLUXNET monitoring network, scalar concentration fluctuations used in eddy covariance measurements of CO_2 and H_2O have relied on one of two classes of high-frequency gas analyzers: open-path analyzers that measure gas concentrations in situ, and traditional closed-path analyzers that draw air from above the canopy through an intake tube to an analyzer housed at some distance from the sampling point. The advantages and shortcomings of each instrument have been well reviewed and documented (Burba et al., 2011; Haslwanter et al., 2009; Leuning and Judd, 1996), and are summarized in Table 1. Briefly, a chief advantage of open-path systems is the relatively small amount of spectral flux attenuation at high frequencies, which can be considerable for traditional closed-path systems requiring long intake tubes. A chief advantage of closed-path systems is that flux terms related to air density fluctuations (i.e. Webb–Pearman–Leuning, or WPL, term, Webb et al., 1980) are small because air temperature fluctuations are effectively damped during travel from the inlet location to the analyzer.

Within the past three years, a new class of enclosed-path analyzers has become available for use in eddy covariance applications. These analyzers are characterized by enclosed designs suitable for outdoor deployment, permitting the analyzers to be co-located with sonic anemometers above the canopy with relatively short (<1 m) intake tubes. Consequently, high-frequency flux attenuation errors common to traditional closed-path designs could be reduced with this new class of analyzers. These analyzers also feature integrated, high-frequency measurements of cell temperature

* Corresponding author. Tel.: +1 812 355 3010.
E-mail address: knovick@indiana.edu (K.A. Novick).

0168-1923/$ – see front matter. Published by Elsevier B.V.
http://dx.doi.org/10.1016/j.agrformet.2013.06.020

Table 1
Some advantages and disadvantages of open-path gas analyzers and traditional closed-path analyzers. The third column describes the expected operational features of the new generation of enclosed, fast-response closed-path analyzers.

	Open-path	Traditional closed-path	New closed-path
High-frequency flux attenuation	Minimal	Large due to interactions with tube walls	Reduction relative to traditional closed-path due to shorter path length
Lag time relative to sonic	Short	Long	Short
Webb–Pearman–Leuning (WPL) terms	Temperature corrections large	Temperature corrections small due to intake tube damping	Unnecessary as the analyzer permits an estimate of instantaneous mixing ratio
Adverse weather performance	Poor performance when sensor is wet	Less data loss during adverse weather	Less data loss during adverse weather
Power requirements	Low	High	Low

and pressure (in addition to gas concentrations), supporting instantaneous measurements of mixing ratio relative to dry air that can be used in raw flux calculations as a strategy to obviate the need for WPL density terms (Leuning, 2004).

There are currently two enclosed, high-frequency closed-path analyzers commercially available for eddy covariance applications: the LI-7200 (Li-Cor, Lincoln, NE, USA, Burba et al., 2011), and the EC155 (Campbell Scientific, Logan, UT, USA). The latter is the focus of this study, which was conducted in a new flux monitoring site located in the complex terrain of the Coweeta Hydrologic Laboratory (Otto, NC, USA). Our primary objective is to assess the extent to which to the magnitude of spectral loss and density corrections are minimized with the EC155. We also evaluate the appropriateness of applying an analytical approach to correct for co-spectral loss to flux records measured with the EC155, and discuss the performance of the EC155 during adverse weather conditions. To our knowledge, this is the first study to describe characteristics of eddy covariance data measured with the EC155, and among the first studies to explore the spectral properties of this new class of enclosed-path analyzers.

2. Theoretical considerations

This study is conducted in a site located in complex terrain and in a challenging environment characterized by frequent occurrence of rain and fog. Accurate estimates mass and energy exchange from this site requires consideration of not only raw turbulent flux measurements, but also storage and advection fluxes which are prominent in complex terrain (Aubinet et al., 2010; Feigenwinter et al., 2004). A full analysis of the turbulent, storage and advective fluxes at this site will be explored in more detail in a future study. The focus here is a comparison of vertical turbulent fluxes of mass and energy measured with a range of gas analyzers, with a particular focus on the spectral and density corrections described in more detail in the following subsections, and on analyzer performance during adverse meteorological conditions. Thus, it is important to note that the turbulent fluxes discussed hereafter do not necessarily represent the total ecosystem fluxes of the scalars of interest, though biases in the fluxes related to storage and advection fluxes should not influence the turbulent flux comparisons, since all instruments are co-located at the same height above the canopy.

2.1. The spectral properties of the measured turbulent fluxes

The measured turbulent flux can be expressed as the integrated co-spectrum of deviations in vertical wind speed (w') and deviations in scalar concentration (ρ_c'), representing mass–density measurements in the case of CO_2 and H_2O, such that:

$$\overline{w'\rho_c'} = \int_0^\infty Co_{wc}(f)df \tag{1}$$

where f is frequency (Hz) and Co_{wc} is the co-spectrum. It is well-known that eddy covariance systems are unable to resolve all turbulent flux-carrying eddies (Massman and Clement, 2004). In particular, they inadequately measure the flux information associated with the smallest (i.e. highest frequency) eddies and largest (i.e. lowest frequency) eddies. Limitations associated with instrument response time, gas sorption on inlet tubes, and separation distances between the sonic anemometers and gas analyzers act as effective low-pass filters. Moreover, Reynolds averaging over a finite time period (typically 30 or 60 min), which is selected as a compromise between resolving the most active eddies responsible for mass and momentum transport and the need for stationary conditions, acts as an effective high-pass filter.

As detailed in the comprehensive review by Massman and Clement (2004), spectral corrections generally fall into one of two distinct categories. The first, termed the "transfer function approach," is a largely analytical approach that relies on a collection of empirical or physically-based transfer functions to estimate both high and low frequency spectral loss. One of the most widely used transfer function frameworks is an analytical approach (Massman, 2000, 2001), hereafter the "M21 approach," that includes transfer functions to correct for instrument line averaging, sonic and gas analyzer lateral and longitudinal separation, tube attenuation for enclosed- and closed-path analyzers, and the high-pass filtering associated with block averaging and detrending. The second approach, termed the "in situ approach," relies on a correction factor that is essentially the ratio of a reference flux (typically sensible heat flux, which is assumed to have little spectral attenuation) to an attenuated flux (Goulden et al., 1997; Hollinger et al., 1999). Table 2 outlines some of the assumptions, advantages, and disadvantages inherent to the M21 versus the "in situ" approach.

One prominent feature of the M21 approach is the assumption that co-spectra can be well represented by the following model:

$$\frac{fCo_{wc}(f)}{\overline{w'\rho_c'}} = \frac{2}{\pi}\frac{f/f_x}{1+\left(f/f_x\right)^2} \tag{2}$$

where f_x is the frequency at which the co-spectra peak. The in-situ approach does not assume, a priori, any particular co-spectral shape. As discussed in Massman and Clement (2004), the application of the M21 approach is most successful in experiments where high-frequency flux attenuation is minimal, and differences between measured co-spectra and the model of Eq. (2) are also small. Traditional closed-path analyzers often rely on long sample tubes to transfer air from inlet locations at the top of the

Table 2
Some characteristics of the M21 and in-situ approaches to spectral correction of measured fluxes.

	M21 analytical approach	*In-situ* approach
Assumptions regarding shape of the co-spectra	Assumes co-spectra can be described by Eq. (4) reasonably well	Assumes co-spectral similarity between the reference and attenuated flux
Computational cost	Low	High
Historically, best applied to. . .	Open-path systems	Closed-path systems
Primary advantage	Comprehensive and largely independent of measured fluxes	Does not rely on an assumed co-spectral shape;
Primary disadvantage	Approach is not appropriate for large high-frequency attenuation	Does not correct for high-frequency attenuation of the reference flux
Reference	Massman (2000, 2001)	Hollinger et al. (1999), Su et al. (2004)

tower to the location of the analyzer at the bottom of the tower. High-frequency fluctuations of trace gases and temperature can be damped in these tubes due to mixing and interactions between the scalars and the tube walls, causing significant deterioration in the frequency response of the analyzer that becomes even more severe as the tubes age (Leuning, 2004; Su et al., 2004).

Consequently, because flux measurements made with open-path systems are not affected by errors associated with tube effects, high-frequency losses tend to be smaller for open- as compared to traditional closed-path analyzers (Leuning and Judd, 1996). The new class of enclosed, fast-response enclosed-path analyzers (e.g. the EC155 and LI-7200) rely on very short intake tubes (i.e. <1 m), which could reduce errors associated with tube effects and facilitate the application of co-spectral correction techniques that rely on assumed co-spectral models (e.g. the M21 approach).

In practice, spectra and co-spectra are often presented as a function of a non-dimensional (or reduced) frequency (n) defined as

$$n = \frac{f(z - d_0)}{\overline{U}} \tag{3}$$

where z is measurement height, d_0 is the zero-plane displacement for momentum (and can differ from those of individual scalars, Siqueira and Katul, 2010) and $\overline{U}$ is mean horizontal wind speed. If n_x is the non-dimensional frequency at which the spectral peak occurs, then with respect to Eq. (2), $f/f_x = n/n_x$. Thus, in this analysis, spectra are often shown as a function of n or n/n_x for consistency with other studies.

The model of Eq. (2) predicts the co-spectra will decay according to a −2 power law in the inertial subrange. Classically, co-spectra are expected to decay according to a −7/3 power law (Kaimal et al., 1972), and while the −2 decay of Eq. (2) may have been selected for the sake of mathematical convenience (Massman, 2000, 2001), some recent work shows experimental evidence for a −2 power law (Bos et al., 2007; Cava and Katul, 2012; Su et al., 2004). In any event, it is also interesting to see how well the measured co-spectra here conform to a more general model given as (Massman and Clement, 2004):

$$fCo(f) = A_0 \frac{n/n_x}{\left[1 + m\left(n/n_x\right)^{2u}\right]^{\frac{1}{2u}\left(\frac{m+1}{m}\right)}} \tag{4}$$

where A_0 is a scaling parameter and m is the inertial subrange slope parameter. For a −7/3 decay, m should assume a value of 3/4. For a −2 decay, m should be 1. The parameter u describes the broadness of the central portion of the co-spectra. For co-spectra similar to the flat-terrain co-spectra described by Kaimal et al. (1972), $u \sim 0.5$. Higher values of u indicate more sharply peaked co-spectra, and lower values of u indicate more broad co-spectra; The broadness of the co-spectra can vary both with atmospheric conditions or from one instrument to the next, and the factors controlling broadness are not explored in this study. Rather, the broadness of a given co-spectrum is simply assessed to determine the suitability of the M21 correction approach, noting that the analytical approach is not particularly sensitive to the value of u except for exceptionally broad or peaked co-spectra (Massman and Clement, 2004).

2.2. Density corrections

Open-path analyzers directly measure the mass–density of CO_2 and H_2O (i.e. ρ_c), a quantity that can be affected by fluctuations in water vapor concentration and temperature, which in turn produce fluctuations in air density. In their seminal paper, Webb, Pearman and Leuning (1980, hereafter WPL) proposed the following formulation to account for these effects on the measured turbulent fluxes

$$F_{C,EC} = \overline{w'\rho'_{cMEAS}}\,(\text{Term I}) + \mu\frac{\rho_c}{\rho_a}\overline{w'\rho'_q}\,(\text{Term II}) + \overline{\rho_c}(1 + \mu\sigma)\frac{\overline{w'T'}}{\overline{T}}\,(\text{Term III}) \tag{5}$$

where $F_{C,EC}$ implies the ecosystem flux measurements associated with the eddy covariance system (as opposed to storage and advection flux estimates which must be derived from vertical and horizontal profiles). The first term on the RHS is the measured vertical turbulent flux, μ is the ratio of the molecular mass of air to the molecular mass of water, ρ_a is the density of dry air, σ is the ratio of water vapor density to dry air density, and $\overline{w'\rho'_q}$ and $\overline{w'T'}$ are measured vertical turbulent fluxes of water vapor and kinematic heat, respectively. Commonly, the second term is called the "water vapor term" and the third term is called the "temperature term." More recent work has suggested that an additional pressure expansion term should also be considered (Lee and Massman, 2011), such that the RHS of Eq. (5) becomes

$$F_{C,EC} = \text{Term I} + \text{Term II} + \text{Term III} - \overline{\rho_c}(1 + \mu\sigma)\frac{\overline{w'p'}}{\overline{p}}\;(\text{Term IV}) \tag{6}$$

where p is atmospheric pressure.

The WPL correction has been widely used and also thoroughly reviewed and vetted (Detto and Katul, 2007; Lee and Massman, 2011; Leuning, 2007; Paw et al., 2000). In general, the theoretical formulation is considered to be quite robust, though errors in the application of the corrections may be introduced if $\overline{w'\rho'_q}$, $\overline{w'T'}$, or other terms in Eqs. (5) and (6) are not accurately measured.

An alternative approach is to calculate turbulent fluxes of trace gases directly from the mixing ratio of the gas, such that $\rho_c = s\rho_a$ and $F_{C,EC} = \rho_a\,(\overline{w's'})$ (Burba et al., 2012) where s is the mixing ratio (mol/mol) relative to dry air and ρ_a is determined from sample cell pressure, temperature, and water vapor concentration measurements. This approach is possible for closed-path analyzers that measure CO_2 and H_2O density, as well as sample pressure and temperature. This approach, hereafter the "mixing ratio approach," has

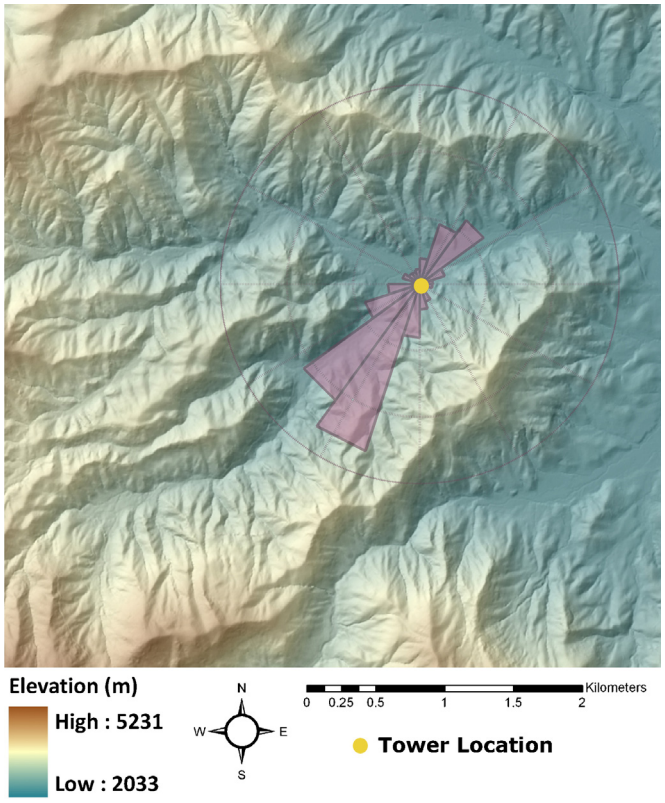

Fig. 1. Elevation surrounding the Coweeta flux tower. The purple bars are a rose plot of wind direction measured at the top of the tower from January to December, 2011.

often been adopted in applications using traditional closed-path systems, though complications arise when one or more of the variables is measured at a different frequency than the others, or when the instrument response time differs considerably for CO_2 and H_2O (Massman and Lee, 2002). These complications have the potential to be alleviated in systems that rely on the new class of fast response, enclosed-path analyzers which measure all four variables at the same frequency.

3. Methods

The experiment was conducted in a ~80 year-old mixed hardwood forest (35.059N, 83.427W, 690 m asl) in the Coweeta Hydrologic Laboratory. Coweeta is located in the southern Appalachians of western NC and is a USDA Forest Service Experimental Forest and National Science Foundation Long-Term Ecological Research Site. The tower is situated in complex, mountainous terrain characterized by a 30% slope within the flux footprint in the SE direction, and local slopes of <10% to the north and west (Fig. 1). Mean annual temperature is 12.9 °C and mean annual precipitation is 1495 mm. The dominant overstory species are *Liriodendron tulipifera*, *Quercus alba*, *Betula lenta*, and *Acer rubrum*, which comprise 24%, 17%, 11% and 8% of the basal area, respectively. The dominant understory species is *Rhododendron maximum*, which comprises 13% of basal area. Preliminary data from an LAI-2000 plant canopy analyzer indicate a peak LAI of ~5.8 m^2 m^{-2}. Mean canopy height is ~28 m.

Eddy covariance measurements were made at the top of the tower beginning in January, 2011, and are described in more detail in the following sub-section. Other above-canopy measurements included air temperature and humidity (HMP45C, Vaisala, Vantaa, Finland), photosynthetically active radiation (LI-190, Li-Cor), and net radiation (CRN4 Net Radiometer, Kipp and Zonen, Delft, the Netherlands).

3.1. Eddy covariance measurements

Long-term eddy covariance measurements were made with an EC155 gas analyzer (Campbell Scientific) and an RMYoung 81000 sonic anemometer (RMYoung, Traverse City, MI, USA) co-located at z = 37 m. In this application, the stainless steel intake tube was 0.58 m and had a diameter of 2.7 mm. Calibrations of the analyzer were performed weekly using an ultra-high purity N_2 zero gas, a 1000 ppm CO_2 span gas (balanced with nitrogen), and a dew point generator (LI-610, Li-Cor Biogeosciences, Lincoln, NE) for water vapor span. Automatic calibration checks were performed daily for the CO_2 zero and span, and drift was observed to be low. Specifically, the mean CO_2 during the zero check was 3.2 ppm (range of −2.3 to 9.4), and the mean CO_2 concentration during the span check was 997 ppm (range of 984 to 1015, or <2%).

At a flow rate of 7 L min^{-1}, air travel time along the tube is theoretically 0.03 s, or less than one scan interval at the measurement frequency of 10 Hz. The EC155 was programmed to use a 20 Hz bandwidth filter, which results in an additional delay of 0.20 s (or two scan intervals) for the gas concentration measurements relative to the sonic anemometer measurements. Lag times were independently determined from a cross-correlation analysis using data collected in May, 2011. For CO_2, the average lag time associated with peak correlation between $w\prime$ and $[CO_2]'$ was 0.1 s. For H_2O, the cross-correlation analysis revealed an average lag time of 0.3–0.4 s. Sources of variability in the H_2O lag are explored in more detail in the results section.

Raw data were collected and stored at 10 Hz, and post-processing was performed with MATLAB (Mathworks, Natick, MA, USA). Coordinate axes of the wind data were rotated using a sector-wise planar-fit (Wilczak et al., 2001) approach, with sectors delineated as follows: (1) Sector 1, wind direction (WD) <40° or >310° clockwise from N, (2) Sector 2, WD between 40°–85° from N, (3) Sector 3, WD between 86°–229° from N, and (4) Sector 4, WD between 230°–310° from N (Fig. 1). These sectors were informed by the relationship between the local topographic slope and the wind angle of attack determined from the sonic anemometer data after a 1D coordinate rotation to align horizontal wind speed with the mean wind direction. All variables were first detrended before calculation of means and turbulent fluxes. As described in Section 3.2, carbon dioxide and water vapor fluxes from the EC155 system were calculated directly from the instantaneous mixing ratio measurements, and again from mass–density concentration measurements. The EC155 outputs concentration measurements as mixing ratio, and mass–density concentrations are determined from the mixing ratio, and sample cell temperature and pressure.

The M21 analytical spectral correction was applied to the flux data. The correction includes time constants for sonic anemometer line averaging (over a 11 cm path length), lateral separation of the sonic anemometer and gas analyzer (with a separation distance of 10 cm), longitudinal separation (with a first order instrument) of the sonic anemometer and gas analyzer (with a separation distance of 10 cm), volume averaging in the analyzer cell (a cylinder with a diameter of 0.79 cm and a length of 12 cm), block averaging, and linear detrending. The M21 corrections rely on an estimate of the intrinsic time constant of the analyzer (τ_1), necessary for estimating the longitudinal separation time constant. Noting that the EC155 operating software employs a digital recursive filter with a bandwidth of 20 Hz, a time constant of τ_1 = 0.05 s was selected. For reference, the time constant of the LI-6262 (Li-Cor), a traditional closed-path analyzer, is typically taken to be τ_1 = 0.1 s (Massman and Clement 2004). M21 spectral corrections were also applied to the sensible heat and momentum fluxes, incorporating sonic

Table 3
Details on the flux comparisons used in this analysis. The number of hourly blocks of data (N) used in each comparison is shown in parentheses. Abbreviations describing data processing as follows: 'PF' denotes a sector-wise planar fit coordinate rotation, '2D' denotes a 2D coordinate rotation, 'MR' denotes fluxes derived from instantaneous mixing ratio, 'MD' denotes fluxes derived from mass density concentration measurements, and 'TF' indicates threshold filtering (i.e. the removal of carbon flux data whose magnitude exceeds 40 μmol m^{-2} s^{-1}, and the removal of water vapor flux data <−1.2 g m^{-2} s^{-1} or >0.40 g m^{-2} s^{-1}). 'PECS-QC' indicates quality control approaches used by the Ameriflux Portable Eddy Covariance System (PECS), including filters for stationarity, turbulence regime, wind direction and angle of attack, and spike detection (see Section 3.2) The relevant figures showing results from each comparison are also listed.

	Date of comparison	Gas analyzers	Processing	Flux abbreviations	Figure(s)
Comparison of enclosed-path fluxes estimated from mixing ratio and mass density concentrations (N = 5855)	1 Jan 2011–31 Dec 2011	EC155 EC155	PF,MR, TF PF,MD, TF	$F_{C,EC155}$, $F_{Q,EC155}$ $F_{C,EC155,MD}$ $F_{Q,EC155,MD}$	Fig. 9
5 month comparison between the enclosed path system and an open path system (N = 1500)	1 Aug 2011–30 Dec 2011	EC155 LI-7500	PF, MR, TF PF, MD, TF	$F_{C,EC155}$, $F_{Q,EC155}$ $F_{C,LI7500}$, $F_{Q,LI7500}$	Figs. 2, 3, 5, 8, 11 and 12
7-day comparison between the enclosed path system and the Ameriflux Portable Eddy Covariance System (PECS) (N = 86)	30 Aug 3011–5 Sept 2011	EC155 LI-7200 LI-7500	2D, MR, PECS-QC 2D, MR, PECS-QC 2D, MR, PECS-QC	$F_{C,EC155,PECS}$ $F_{Q,EC155,PECS}$ $F_{C,LI7200,PECS}$, $F_{Q,LI7200,PECS}$ $F_{C,LI7500,PECS}$, $F_{Q,LI7500,PECS}$	Fig. 10

anemometer line averaging effects. The maximum frequency f_x (see Eq. (2)) was specified as a function of the atmospheric stability parameter after estimating f_x using non-linear regression of co-spectra ensemble-averaged into discrete frequency bins (data not shown). The atmospheric stability parameter ζ was calculated as $\zeta = (z - d_0)/L$, where L is the Obukhov length. Appropriate WPL terms were applied to the fluxes after the spectral correction to estimate $F_{C,EC}$.

A conservative post-processing quality control approach was applied. Specifically, data were screened only to remove CO_2 flux measurements with absolute magnitudes in excess of 40 μmol m^{-2} s^{-1}, and water vapor flux estimates less than −0.12 g m^{-2} s^{-1} and greater than 0.4 g m^{-2} s^{-1}. In some cases, a standard friction velocity filter was also applied whereby data collected when $u^* < 0.25$ m s^{-1} were removed from the data records. We note that a more rigorous assessment of the suitability of a u^* quality control for these data is the focus of other work; here, this simple filter was employed to determine to what extent biases observed in the flux records are limited to data characterized by low or insufficient turbulence.

3.2. Eddy covariance measurements for flux comparisons

This analysis relies on several flux comparisons, which are summarized in Table 3. First, mixing-ratio derived fluxes from the EC155 where compared to those derived from EC155 mass–density scalar concentration measurements using an approach similar to that described in Burba et al. (2012). Specifically, carbon and water vapor fluxes were calculated directly from the mixing ratio (i.e. $F_{C,EC155}$ and $F_{Q,EC155}$) and from the mass density (i.e. $F_{C,EC155,MD}$ and $F_{Q,EC155,MD}$) with the WPL terms of Eqs. (5) and (6) calculated using temperature and pressure fluctuations measured in the sample cell.

The EC155 mixing ratio fluxes were also compared to fluxes estimated from a co-located open-path system comprised of an LI-7500 infrared gas analyzer (Li-Cor) and an RMYoung 81000 sonic anemometer deployed for five months from August–December, 2011. A field calibration of the LI-7500 was performed immediately before and immediately after its deployment. Offset errors in the concentration measurements between the EC155 and the LI-7500 were observed (on the order of 25 mg CO_2 m^{-3} and −3 to 3 g H_2O m^{-3} depending on time). The LI-7500 concentrations were corrected for these bias errors. After this correction, regression coefficients for scalar concentrations and wind variables between the two systems were as follows, with standard error estimates on regression coefficients shown in parentheses.

$$\begin{cases} CO_{2[EC155]} = 0.99(0.01)CO_{2[LI-7500]} + 0.85(5.5) \quad [\text{mg m}^{-3}] \\ H_2O_{[EC155]} = 1.01(0.01)H_2O_{[LI-7500]} - 1.68(0.1) \quad [\text{g m}^{-3}] \\ u_{[RMYoung]} = 0.99(0.01)u_{[CSAT3]} + 0.025(.001) \quad [\text{m s}^{-1}] \\ w_{[RMYoung]} = 0.96(0.01)w_{[CSAT3]} + 0.028(.001) \quad [\text{m s}^{-1}] \\ T_{[RMYoung]} = 0.995(0.001)T_{[CSAT3]} - 0.201(0.024) \quad [^\circ\text{C}] \end{cases} \tag{7}$$

Again, the RMYoung sonic is the sonic associated with the EC155, and the CSAT3 sonic is the sonic associated with the LI-7500. The relative errors in these data (≤5%) are consistent with those reported in a recent study synthesizing the results of eddy covariance cross-system comparisons from over 80 different sites (Schmidt et al., 2012).

A sector-wise, planar-fit coordinate rotation was applied to the open-path system with unique rotation coefficients. The M21 spectral correction was also applied to open-path system fluxes, with time constants for sonic anemometer line averaging, lateral and longitudinal separation (without a first order instrument), and volume averaging (for a cylinder with a length of 0.15 m and a diameter of 16 mm). The magnitude of the M21 corrections was, on average, slightly higher for the EC155 system ($\langle M21_{EC155} - M21_{LI7500} \rangle$ = 0.1 μmol m^{-2} s^{-1} for CO_2 flux), but in general the corrections for the open and closed-path systems were similar and rarely exceeded 12% of the raw turbulent flux.

WPL terms were also applied to the open-path system fluxes, with temperature fluctuations measured by the associated sonic anemometer. The pressure term (see Eq. (6)) for the open-path system was calculated using the ambient pressure measured with the LI-7500, and may be sensitive to artificial variations in pressure related to wake effects as air travels over the spar poles of the analyzer. However, we note that the statistics of the pressure term for the open-path and enclosed-path systems do not suggest large contamination by these errors. The mean value of the pressure term for CO_2 flux was near zero for both systems ($\langle \text{Term IV} \rangle$ = −.0270 and .0276 μmol m^{-2} s^{-1} for the EC155 and open-path systems, respectively) and the variance was lower for the open-path system (S.D. = .251 and .111 μmol m^{-2} s^{-1} for the

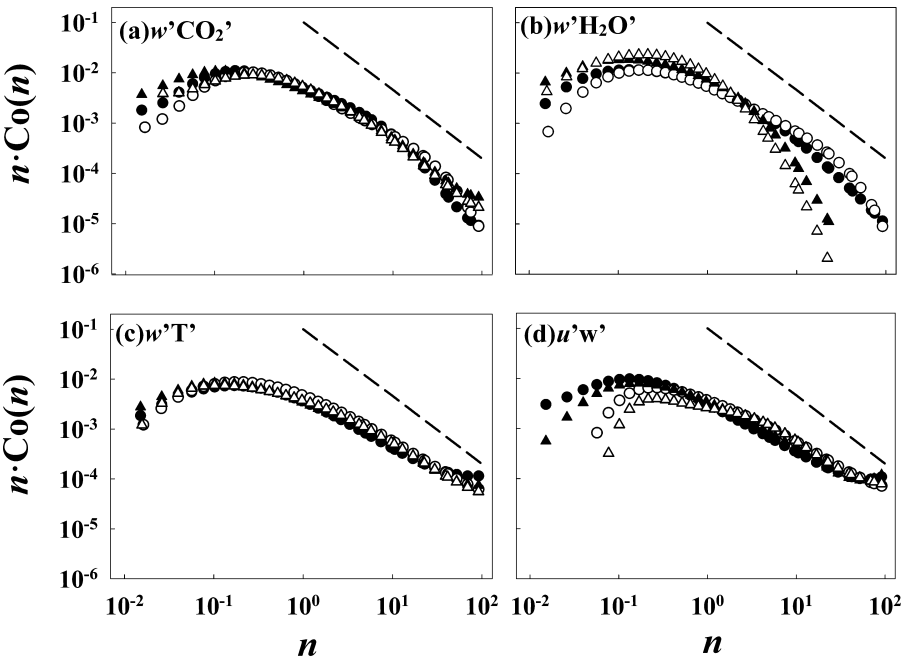

Fig. 2. Ensemble average and smoothed co-spectra using (a) CO_2 flux, (b) H_2O flux, (c) kinematic heat flux, and (d) momentum flux shown as a function of non-dimensional frequency. In (a) and (b), triangles show data with the EC155, and circles show data measured with an LI-7500 open-path gas analyzer (deployed from 1 August 2011 to 30 November 2011). The data in (c) and (d) show data collected the RMYoung sonic anemometers co-located with the EC155 (again, solid squares) and the LI7500 (open-triangles). Closed symbols show data collected during near-neutral conditions ($(-0.2 < \zeta < 0.1)$. Open symbols show data collected during stable conditions ($\zeta > 0.1$). The dashed line indicates a −7/3 spectral decay for reference.

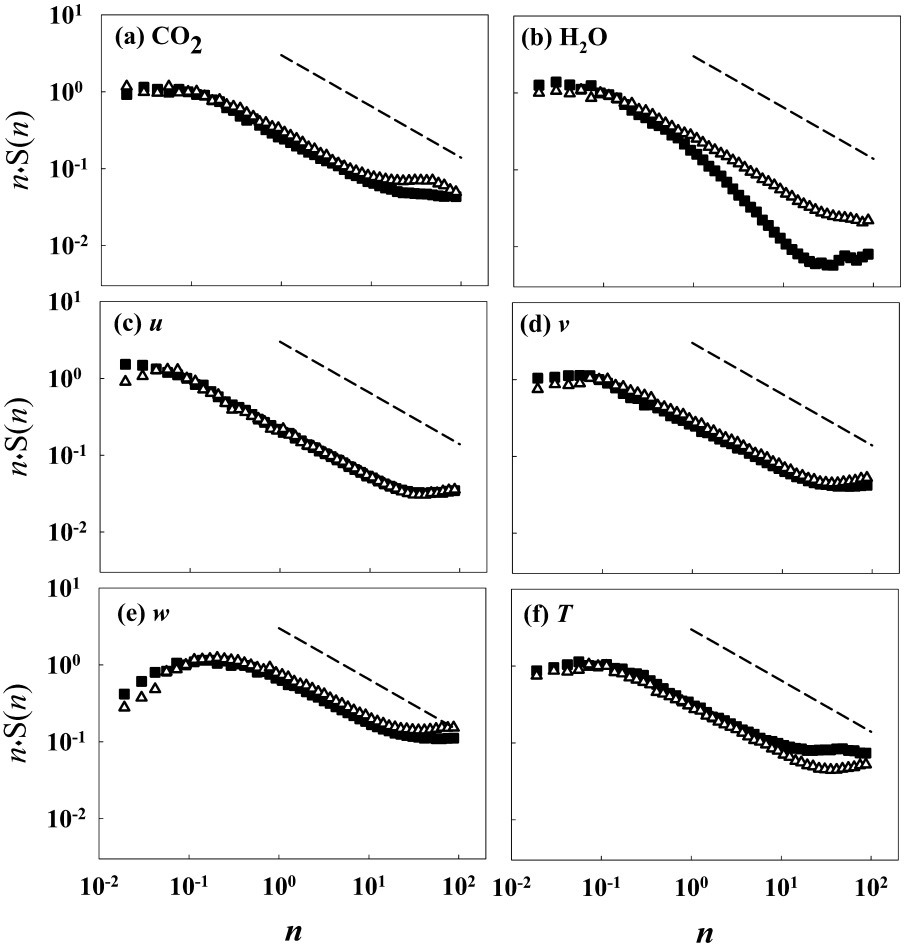

Fig. 3. Ensemble-averaged power spectra normalized by the spectral magnitude at $n = 1$, where n is non-dimensional frequency. Panels (a) and (b) show spectra for carbon dioxide and water vapor concentration for the EC155 (solid squares) and a co-located LI7500 (open-triangles). Each gas analyzer is linked to a separate RMYoung 81000 sonic anemometer, and panels ((c)–(f)) show wind components and virtual temperature for the sonic associated with the EC155 (again, solid squares) and the LI7500 (open-triangles). The dotted line indicates a −5/3 spectral decay for reference.

EC155 and open-path systems, respectively). As was the case with the EC155 fluxes, the only post-processing quality control step was to remove CO_2 flux measurements with absolute magnitudes in excess of 40 μmol m^{-2} s^{-1}, and water vapor flux–flux estimates less than −0.12 g m^{-2} s^{-1} and greater than 0.40 g m^{-2} s^{-1}.

Finally, for seven days in the late summer of 2011, the AmeriFlux Portable Eddy Covariance Station (PECS), part of the AmeriFlux Quality Assurance and Quality Control Intercomparisons program, was deployed on the tower, again at a measurement height of 37 m. Turbulent fluxes were computed using a CSAT3 sonic anemometer (Campbell Scientific) co-located with an LI-7500 open-path analyzer and an LI-7200 fast-response closed-path analyzer. For this comparison, data processing procedures for the EC155 flux data were adjusted to match the protocols of the PECS. Specifically, a 2D coordinate rotation was used instead of the planar fit rotation, and time series were not detrended before covariances were calculated. During the comparison period, data from all systems were quality controlled based on criteria for stationarity, well-developed turbulence, and wind direction relative to sonic orientation (Foken et al., 2004). In addition, periods when more than 10% of the high frequency data were excluded by spike detection or instrument flags were not included in the comparison.

3.3. Spectra and ogive calculations

Co-spectra were calculated using hourly blocks of data, with the time series truncated to a length of 2^{15} (or 32768, noting that each hourly averaging period contains 36000 data points), and data were not zero-padded. The spectra were smoothed using a window that expands with frequency, and then normalized by the area under the curve and ensemble averaged within discrete frequency bins after first discarding the extreme 10% of data points within each bin. The parameters of Eq. (4) were fit using nonlinear least-squares regression using only the central portion of the ensemble-averaged co-spectra to avoid a situation where co-spectral loss at high frequencies would affect estimates of inertial subrange decay. Parameters were fit for two stability classes: near-neutral ($-0.2 < \zeta < 0.1$, where ζ is the non-dimensional stability parameter) and stable ($\zeta > 0.1$). Co-spectra were calculated as functions of both the non-dimensional frequency n and dimensional frequency f.

Co-spectra were also calculated using 240-min blocks of data to create ogives, or integrated co-spectra. They are typically used to determine the optimal averaging period; here we also use ogives to quantify water vapor flux loss related to high-frequency spectral attenuation in the enclosed as compared to open-path analyzer.

Finally, to evaluate the timescales of variations for the principle scalars (CO_2, H_2O, the three Cartesian wind speed components u, v, and w, and T) independently of the co-spectral comparison, ensemble-average power spectra were calculated in a manner similar to the co-spectra. To facilitate cross-instrument comparisons, the ensemble average spectra were normalized by their magnitude at $n = 1$.

3.4. Estimating artificial self-heating of the LI-7500

There is a growing body of work suggesting that flux records from open-path systems may be infected with errors related to open-path instrument heating (Burba et al., 2012; Reverter et al., 2011). Instrument heating artifacts can produce an apparent heat flux in the open-path control volume that is not sensed by the sonic anemometer. The WPL temperature term (i.e. Term III of Eq. (5)) may be adjusted to include this heating effect via

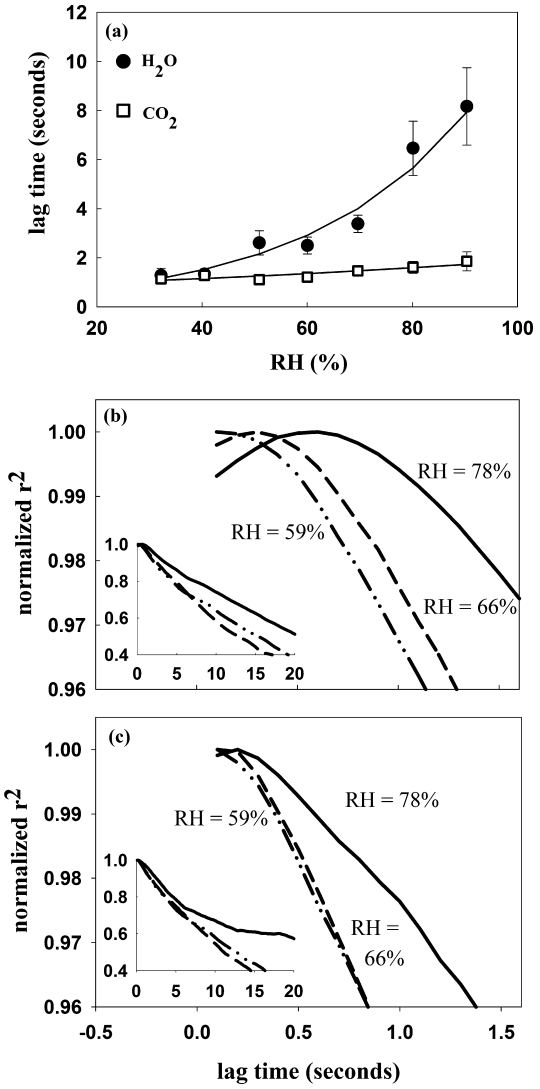

Fig. 4. The average tube lag time associated with peak correlation between deviations in vertical wind velocity (w') and deviations in CO_2 concentration (open squares), and between deviations in vertical wind velocity (w') and deviations in H_2O concentration (solid circles) as a function of relative humidity (RH) (panel a). Data represent mean lag times within discrete RH classes using data collected in May, 2011. Error bars show the standard deviation of the mean. Panels (b) and (c) show three typical lagged correlation plots for H_2O (b) and CO_2 (c) generated from hourly blocks of data collected in the morning of June 29, 2011, when RH decreased from 77% (0900–1000 h) to 59% (1100–1200 h). The mean RH during each hourly block is shown on the figure. The y-axes shows normalized correlation coefficients (i.e. r^2 divided by the maximum correlation in each hourly block). The inset shows the same functions over a longer range of lag time.

$$(\text{Term III})_{ADJ} = \overline{\rho_c}(1+\mu\sigma)\frac{\left(\overline{w'T'} + \overline{w'T'}_{\text{SENSOR}}\right)}{\overline{T}} = \text{Term III} + \overline{\rho_c}(1+\mu\sigma)\frac{\left(\overline{w'T'}_{\text{SENSOR}}\right)}{\overline{T}}, \quad (\text{Term V}) \tag{8}$$

where $\overline{w'T'}_{\text{SENSOR}}$ is the apparent heat flux produced by instrument heating, T is sonic temperature, and Term V (the last term on the RHS of the equation) is the difference between the traditional WPL temperature correction term and $(\text{Term III})_{ADJ}$. We estimated Term V using the equations presented in Burba et al. (2008), which relate the apparent heat flux to the temperature of the instrument's bottom window, top window, and spar poles, which in turn are estimated from meteorological variables like air temperature,

Table 4
Parameters for the model of Eq. (4), estimated from non-linear regression with the ensemble-average co-spectra shown in Fig. 2. The stability classes are near-neutral ($-0.2 < \zeta < 0.1$) and stable ($\zeta > 0.1$).

Variable	Instrument(s)	Stability	A_0	μ	n_x	m
$w'CO_2'$	EC155, RMYoung 81000	Near-neutral	0.044	0.46	0.14	0.86
$w'CO_2'$	EC155, RMYoung 81000	Stable	0.037	0.45	0.25	0.74
$w'CO_2'$	LI-7500, RMYoung 81000	Near-neutral	0.041	0.46	0.22	0.74
$w'CO_2'$	LI-7500, RMYoung 81000	Stable	0.031	0.55	0.27	0.65
$w'CO_2'$	EC155, RMYoung 81000	Near-neutral	0.0868	0.419	0.136	0.74
$w'H_2O'$	EC155, RMYoung 81000	Stable	0.065	0.659	0.196	0.68
$w'H_2O'$	LI-7500, RMYoung 81000	Near-neutral	0.056	0.419	0.163	0.79
$w'H_2O'$	LI-7500, RMYoung 81000	Stable	0.039	0.521	0.21	0.77
$w'T'$	RMYoung 81000	Near-neutral	0.0346	0.46	0.138	0.87
$w'T'$	RMYoung 81000	Stable	0.0341	0.455	0.18	0.80
$w'T'$	RMYoung 81000	Near-neutral	0.0377	0.395	0.17	0.75
$w'T'$	RMYoung 81000	Stable	0.043	0.402	0.212	0.74
$u'w'$	RMYoung 81000	Near-neutral	0.0282	0.492	0.187	0.75
$u'w'$	RMYoung 81000	Stable	0.023	0.321	0.616	0.67
$u'w'$	RMYoung 81000	Near-neutral	0.0365	0.477	0.135	0.74
$u'w'$	RMYoung 81000	Stable	0.019	0.536	0.394	0.68

wind speed, and radiation. We note that the Burba et al. (2008) corrections may not necessarily be universal across sites.

4. Results

4.1. Co-spectra of CO_2, H_2O, heat, and momentum fluxes

The ensemble-averaged CO_2 co-spectra measured with the EC155 and the LI7500 were similar to each other and to the measured co-spectra for sensible heat and momentum (Fig. 2). In the inertial subrange, fluxes generally conformed to a −7/3 power law decay, as confirmed by the magnitude of the derived slope parameter m, which was close to 3/4 (corresponding to a −7/3 decay) in most cases (Table 4). Some high-frequency CO_2 flux loss was apparent in both flux records (Fig. 2a), though again the magnitude of this attenuation was similar for both the open- and enclosed-path systems. Peak frequencies (i.e. n_x) shifted toward higher values for data collected under stable as compared to near-neutral conditions (Table 4), consistent with the classical Kaimal spectra for flat terrain. For most co-spectra, the broadness parameter u was between 0.4 and 0.5 (Table 4).

The co-spectra for heat and momentum fluxes, but not CO_2 and H_2O fluxes, flatten at high frequencies (Fig. 2). The power spectra for all wind and scalar variables exhibit flattening at high frequencies (Fig. 3), which is indicative of white noise introduced by the instruments or the datalogger. That fact that the high-frequency autocorrelation is not evident in the co-spectra for carbon and water fluxes could indicate the action of processes like volume-averaging in the analyzer sample cell and effective high-pass filtering due to horizontal and vertical separation between the analyzer and the sonic. These processes produce high-frequency attenuation counteracting spectral flattening from white noise which would not be realized in the heat and momentum flux records.

In the case of the H_2O fluxes, a more significant amount of high-frequency flux attenuation was observed for the flux records measured with the EC155 system (Fig. 2b). Examination of the power spectra (Fig. 3) showed that the EC155 flux attenuation was driven primarily by differences in the performance of the gas analyzers. At high frequencies, the EC155 CO_2 power spectra was marginally lower than the LI7500 CO_2 power spectra (Fig. 3a), but the EC155 H_2O power spectra was much lower than the LI7500 H_2O power spectra (Fig. 3b). The spectra for the wind components and virtual temperature were generally similar for the two systems (Fig. 3c–f), which is not surprising as the sonics associated with the EC155 and LI7500 are both RMYoung 81000 instruments. Nonetheless, some differences in the vertical velocity and sonic temperature power spectra were evident at high frequencies (Fig. 3e,f). All power spectra generally conformed to a classically predicted −5/3 scaling regime.

The EC155 H_2O flux attenuation at high-frequencies was related to ambient relative humidity (RH). For CO_2' and H_2O', the lag time to peak correlation with w' was exponentially related to RH ($r^2 = 0.96$ and 0.83 for CO_2 and H_2O, respectively, Fig. 4). However, the absolute change in CO_2 lag time was small across the relative humidity gradient (<0.1 s), whereas the H_2O lag increased from ~0.1 s when RH < 50%, to nearly 1 s when RH exceeded 90%.

The model of M21 (i.e. Eq. (2)) appears to be a reasonable model for the measured co-spectra (Fig. 5). The CO_2 flux data from the EC155 and the LI-7500 were well represented by the model (Fig. 5a), at least for frequencies less than 100 $\left(n/n_x\right)$. Greater high-frequency spectral loss for the EC155 H_2O fluxes was again apparent (Fig. 5b). In the inertial-subrange and at low frequencies, the co-spectra for sensible heat (Fig. 5c) were also well represented by the model, though the measured spectra were broader than the model in the range of frequencies close to n_x. Momentum fluxes were well matched to the model for near-neutral conditions (Fig. 5d), with a significant shift toward higher peak frequencies observed for stable conditions.

Integrated co-spectra, or ogive curves, provided additional information about spectral loss at both low and high frequencies. First, an ogive analysis demonstrated that a 60-min averaging period (as compared to a 30-min averaging period) may be most appropriate at this site (Fig. 6). In many cases, stationarity in the magnitude of the ogive curves was reached at frequencies smaller than 3×10^{-4} Hz (which is the minimum frequency resolvable with an hourly averaging period). In other cases, stationarity was achieved at frequencies greater than the minimum frequency resolvable with a half-hourly averaging period. Occasionally, a small amount of flux was contributed by eddies that operate on time scales longer than 120 min (Fig. 6).

The ogive analysis also revealed that the H_2O spectral flux loss at high frequencies represented a relatively small portion of the total water vapor flux. When the ogives shown in Fig. 6 were ensemble averaged and normalized by the total flux magnitude, it was evident that less than 5% of the total H_2O flux was generated by eddies with frequencies greater than n = 1.5 (Fig. 7). Moreover, less than 2% of the total H_2O flux was generated by eddies with frequencies greater than n = 2.

4.2. WPL density terms

The magnitude of the turbulent fluxes of CO_2 measured with the EC155 using the mass-density approach well exceeded the

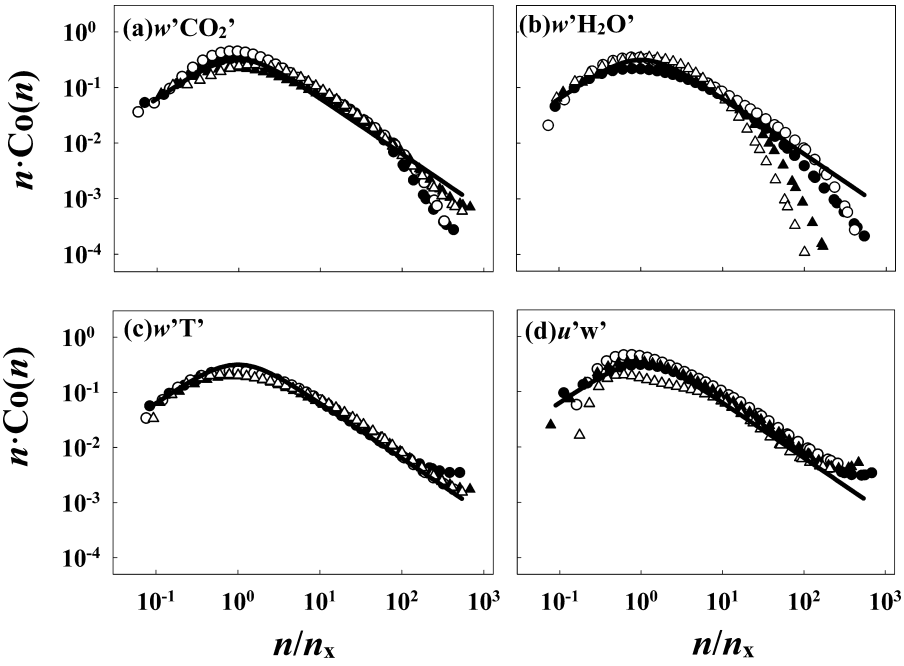

Fig. 5. Same as Fig. 2, except data are shown as a function of normalized frequency, where n_x is the frequency at which the spectra peak (see Table 4). The solid lines show the M21 co-spectra model (i.e. Eq. (2)).

magnitude of the relevant water vapor and temperature WPL terms (i.e. Terms II and III of Eq. (5), Fig. 8a). However, neither the water vapor or temperature terms were negligible, suggesting that the relatively short intake tube length of the EC155 did not effectively damp temperature fluctuations. This result is consistent with previous work suggesting that in order for temperature fluctuations to be completely dampened, the length of the intake tube should be 1000× the diameter of the tube (Rannik et al., 1997). In our case, the length of the intake tube (0.58 m) is ~200× the tube diameter. After the WPL terms (Terms I–IV) were applied, the $F_{C,EC155}$ and $F_{C,EC155,MD}$ agreed well (r^2 = 0.99, $F_{C,EC155}$ = 0.99 $F_{C,EC155,MD}$ − .01 [μmol m^{-2} s^{-1}], Fig. 9a). Before the WPL terms were applied, a clear bias existed in the $F_{C,EC155,MD}$ data (r^2 = 0.93, $F_{C,EC155}$ = 0.87 $F_{C,EC155,MD}$ − .11 [μmol m^{-2} s^{-1}], Fig. 9a). In the case of the open-path system, the density term for temperature fluctuations (i.e. Term III) was large relative to the measured turbulent flux (Fig. 8b).

The time series for the WPL pressure term (Term IV) is not shown on Fig. 8 as its magnitude is very small; however, over the entire length of the available data record, the $F_{C,EC155,MD}$ flux record was overestimated by about 16 g C, or about 3% of the total flux, before the WPL pressure term was applied (Fig. 9b). After accounting for pressure fluctuations, the cumulative bias between the $F_{C,EC155,MD}$ and $F_{C,EC155}$ flux was 3 g C m^{-2}, or essentially negligible.

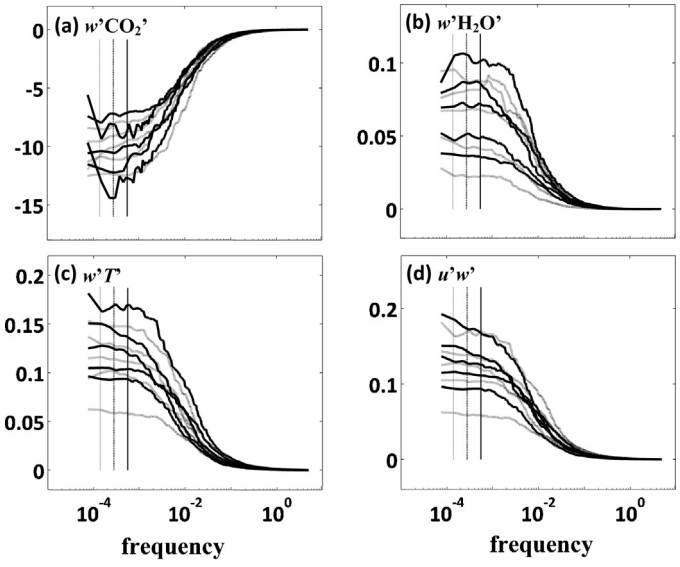

Fig. 6. Ogive curves for (a) CO_2 flux, (b) H_2O flux, (c) kinematic heat flux, and (d) momentum flux. Each line represents the integrated co-spectra associated with one 4 h long block of data collected from 0800 to 1200 EST in early May, 2011. The vertical dashed lines show, in order from left to right, the frequency associated with a 120, 60, and 30 min averaging period. Some ogives are shown in gray to facilitate visual inspection of the data. Units are μmol m^{-2} s^{-1}, g m^{-2} s^{-1}, K m s^{-1}, and m^2 s^{-2} for panels (a), (b), (c), and (d), respectively.

4.3. Cross-system flux comparisons

The EC155 flux records generally compared favorably to fluxes measured with the PECS LI-7200 (Fig. 10a,b) after the quality control filters described in Section 3.1 were applied. For water vapor

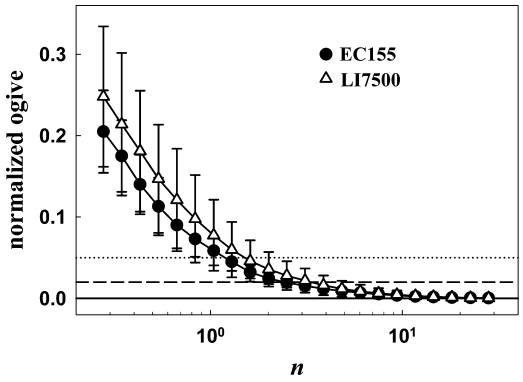

Fig. 7. The high-frequency portion of ensemble averaged and normalized ogive curves for the H_2O flux measured with the EC155 (triangles) and LI-7500 (squares). The solid, dashed, and dotted horizontal lines are drawn at 0.01, 0.02, and 0.05, respectively.

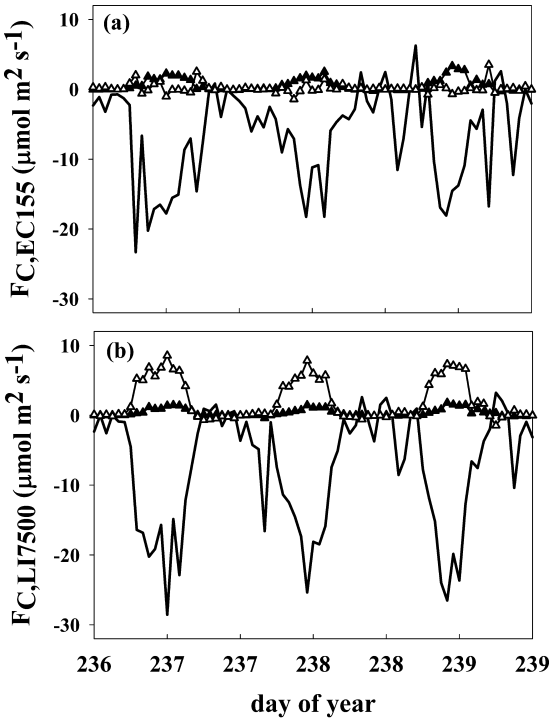

Fig. 8. Time series of raw measured turbulent fluxes (i.e. Term I of Eq. (5), solid lines), the Webb–Pearman–Leuning (WPL) water vapor flux correction (i.e. Term II of Eq. (5), solid triangles), and the WPL temperature flux correction (i.e. Term III of Eq. (5), open triangles). Panel (a) shows data from the EC155 system estimated using the mass density concentration measurements, and panel (b) shows data from the LI-7500 system.

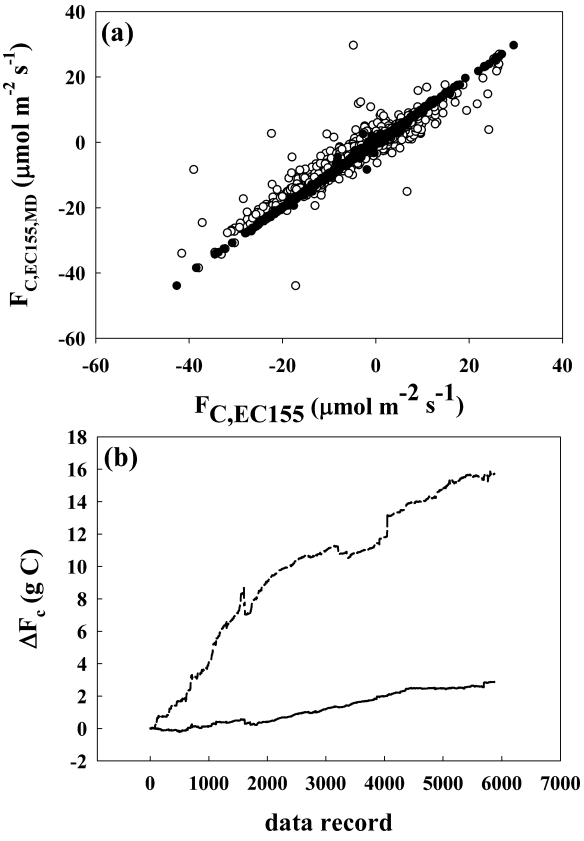

Fig. 9. The top panel shows agreement between the EC155 system CO_2 fluxes derived from the mixing ratio approach ($F_{C,EC155}$) and the mass-density approach ($F_{C,EC155,MD}$) before WPL terms were applied (open circles, $y = -0.87x - .01$ [$\mu mol\,m^{-2}\,s^{-1}$], $r^2 = 0.93$) and after WPL terms were applied (closed circles, $y = 0.99x - .01$ [$\mu mol\,m^{-2}\,s^{-1}$], $r^2 > 0.99$). The bottom panel shows the cumulative difference between the $F_{C,EC155,MD}$ and $F_{C,EC155}$ flux records before (dashed line) and after (solid line) the WPL pressure term (i.e. Term IV in Eq. (6)) was applied to the $F_{C,EC155,MD}$ record.

fluxes, correlation was strong ($r^2 = 0.98$) and biases were small ($F_{Q,EC155,2D} = 0.98F_{Q,LI7200,PECS} - 0.00009$ [$g\,m^{-2}\,s^{-1}$]) for the duration of the five-day comparison period. Correlation was weaker for the CO_2 flux comparison ($r^2 = 0.83$), though again biases were small ($F_{C,EC155,2D} = 0.99F_{C,LI7200,PECS} + 0.77$ [$\mu mol\,m^{-2}\,s^{-1}$]). Agreement between the EC155 fluxes and those measured with the PECS LI-7500 open-path system was less favorable (Fig. 10c,d), with lower correlation and slopes that differed significantly from 1.

With respect to the LI-7500 system co-located with the EC155 for the five-month comparison period, the EC155 underestimated carbon fluxes ($r^2 = 0.94$, $F_{C,EC155} - 0.87F_{C,LI7500} - 0.77$ [$\mu mol\,m^{-2}\,s^{-1}$], Fig. 11a) and water vapor fluxes ($r^2 = 0.94$, $F_{Q,EC155} = 0.88F_{Q,LI7500} + 0.00086$ [$g\,m^{-2}\,s^{-1}$], Fig. 11b). However, agreement between the two systems was dependent on wind and temperature regime. The magnitude of the difference between these two carbon fluxes records (ΔF_c) increased as a function of the angle of attack of the un-rotated wind speed (α), which is defined as the inverse tangent of the ratio of vertical to horizontal wind speed (Fig. 11e). When α was high, the open-path system overestimated fluxes relative to the enclosed-path system. The difference ΔF_c was also related to Term V of Eq. (8), which is the estimated correction for LI-7500 instrument heating (Fig. 11f). Variations in Term V explained about 50% of the variation in ΔF_c when the data were aggregated to binned averages (Fig. 11f), though Term V tended to over-predict the absolute magnitude of ΔF_c ($\Delta F_c = 0.46$[Term V] + 0.13).

The cross-system relationships between mean hourly-averaged CO_2, the standard deviation of hourly-averaged w, and the standard deviation of hourly-averaged CO_2 were either unaffected or improved when α was limited to high values ($\alpha > 5^\circ$, Fig. 12a–c); however, when α was high, the mean w measured by the EC155 was underestimated with respect to the w measured by the LI-7500 (Fig. 12d). Since the $w'C'$ covariance is related to the correlation between w' and CO_2' and the standard deviations of w' and CO_2', the bias in w observed for high α may contribute to the observed bias in measured carbon fluxes at high α (i.e. Fig. 11c).

After the application of the u^* filter, cross-system agreement for carbon flux ($r^2 = 0.94$, $F_{C,EC155} = 0.96$ $F_{C,LI7500} - 0.89$, Fig. 11b) and water vapor flux ($r^2 = 0.98$, $F_{Q,EC155} = 1.05$ $F_{Q,LIy500} - 0.014$, Fig. 11d) measurements improved considerably. Applying the u^* filter removed much of the data characterized by high α ($\langle|\alpha|\rangle = 6^\circ$ for all data and $\langle|\alpha|\rangle = 3.6^\circ$ when $u^* > 0.25\,m^2\,m^{-2}$, with the brackets indicated ensemble averaging over all data). Additionally, the relationship between ΔF_c and Term V disappeared after u^* filtering ($r^2 = .02$)

4.4. Instrument performance during early morning

Large errors in LI-7500 gas concentration measurements were frequently observed during early to mid-morning periods (Fig. 13a). In general, these errors were observed when relative humidity was >90% (Fig. 13b) and the difference between incident and outgoing longwave radiation (ΔR_L, Fig. 13c) was small, which are meteorological conditions associated with dew formation and fog development. For the period of comparison shown in Fig. 13, shortwave radiation (R_S) increased rapidly during the morning periods associated with the anomalies in LI-7500 CO_2 concentration, and no precipitation was recorded at a nearby climate station, suggesting the errors were not caused by rain events. The errors were observed in the open-path CO_2 records for approximately 50% of the nights

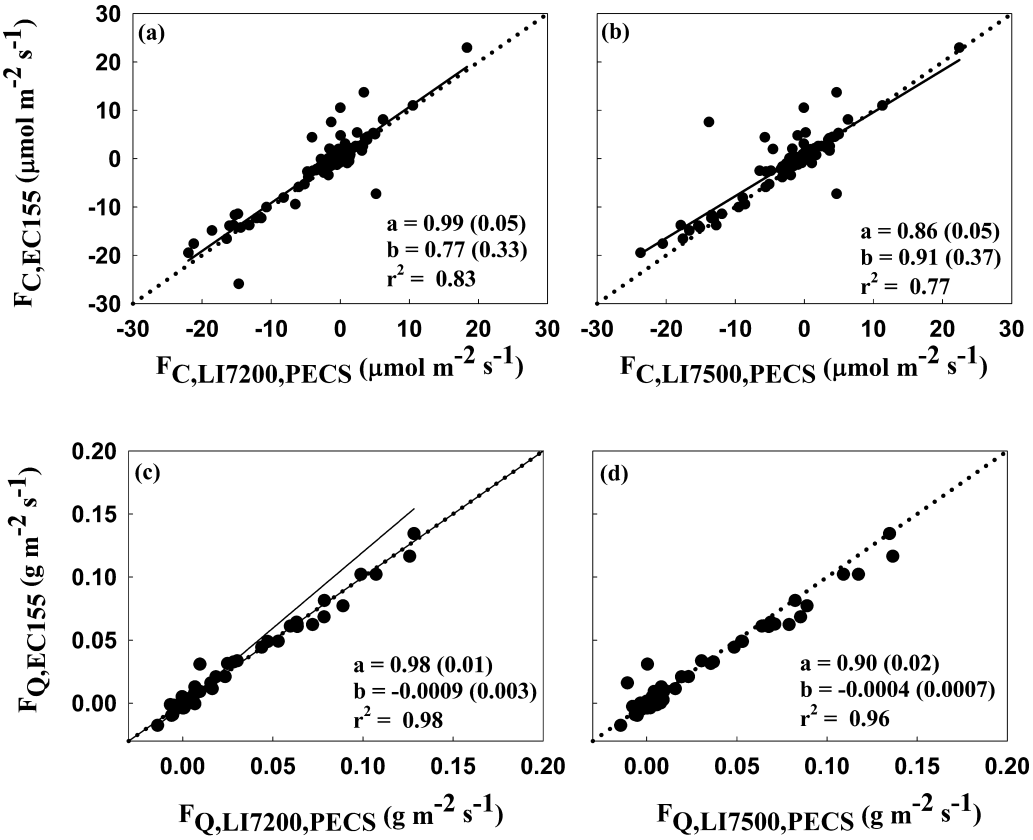

Fig. 10. Agreement between CO_2 flux ((a), (b)) and water vapor flux ((c), (d)) measurements from the EC155 system and the AmeriFlux Portable Eddy Covariance Station (PECS) system. Panels on the left show comparisons between the EC155 flux records and the PECS LI-7200 flux records, and panels on the right show comparisons between the EC155 flux records and the PECS LI-7500 flux records. Descriptive statistics for the parameters of the regression line $y = ax + b$ are shown in each subplot, with the standard error for a and b given in parentheses.

during the study period (8/3/2011 to 12/15/2011). Similar errors were not observed in CO_2 records from the EC155 (Fig. 13a). We did not observe evidence of sonic anemometer malfunctioning during high-humidity periods.

5. Discussion

The new eddy covariance tower at the Coweeta Hydrologic Laboratory relies on an eddy covariance system comprised of a high-frequency, enclosed-path gas analyzer (e.g. the EC155) which is one of a new class of infrared gas analyzers designed to incorporate the advantages of traditional open and closed-path systems, while minimizing disadvantages (see Table 1). This study focused on field performance of the EC155, with particular attention paid to the co-spectral properties of measured fluxes, and the magnitude and biases of flux records calculated using the mixing ratio approach and the more traditional mass–density approach.

We found that high-frequency flux attenuation was minimal for the EC155 CO_2 flux records, and small for the EC155 H_2O flux records. We also showed that EC155 fluxes estimated directly from the mixing ratio agreed very well with fluxes estimated from mass–density after the WPL terms were applied. Flux records measured with co-located open-path systems were biased when compared to the EC155 flux records, though some explanations for these biases are available (as described below). Finally, we demonstrated that the EC155 performs better than the LI-7500 during high-humidity, early-morning periods which are likely characterized by fog events.

These results are relevant to other eddy covariance research efforts, and in particular those efforts relying on new flux monitoring experiment or reviewing data records for potential biases (for example, biases between open- and closed-path instruments). This analysis is also a necessary first step in developing the quality control and flux processing procedures for the new Coweeta eddy covariance tower, which are challenged by complex topography and frequent rain and fog events. Indeed, ongoing work to estimate the contribution of storage and advection fluxes to total ecosystem fluxes in this study site relies on data streams from a number of eddy covariance systems comprised of both open- and closed- path analyzers, and evaluating cross-system biases is necessary before using these data to characterize advection regimes.

5.1. EC155 instrument performance: Lag times, high-frequency flux attenuation, and poor-weather performance

The empirically determined tube lag time for CO_2 (from the maximum correlation analysis) was ~0.1–0.2 s (Fig. 4). For H_2O, the actual tube lag time was close to 0.1 s at low humidity, and then increased exponentially to nearly 1 s at high humidity (Fig. 4). The longer lag time and broader correlation plots when humidity is high likely reflect increased interactions between H_2O molecules and tube walls (Ibrom et al., 2007; Leuning and Judd, 1996; Mammarella et al., 2012; Massman and Ibrom, 2008), and for future analyses, specifying the H_2O lag time as a function of RH may a better strategy than adopting a static lag time. In any event, the observed lag times for this analyzer (~0.1 s for CO_2, and ~0.1 to ~1.4 s for H_2O) are much shorter than those associated with traditional closed-path analyzers, which can exceed 5 s (Schmid et al., 2000).

The CO_2 flux co-spectra measured with the EC155 were similar in shape to those measured with a co-located open-path

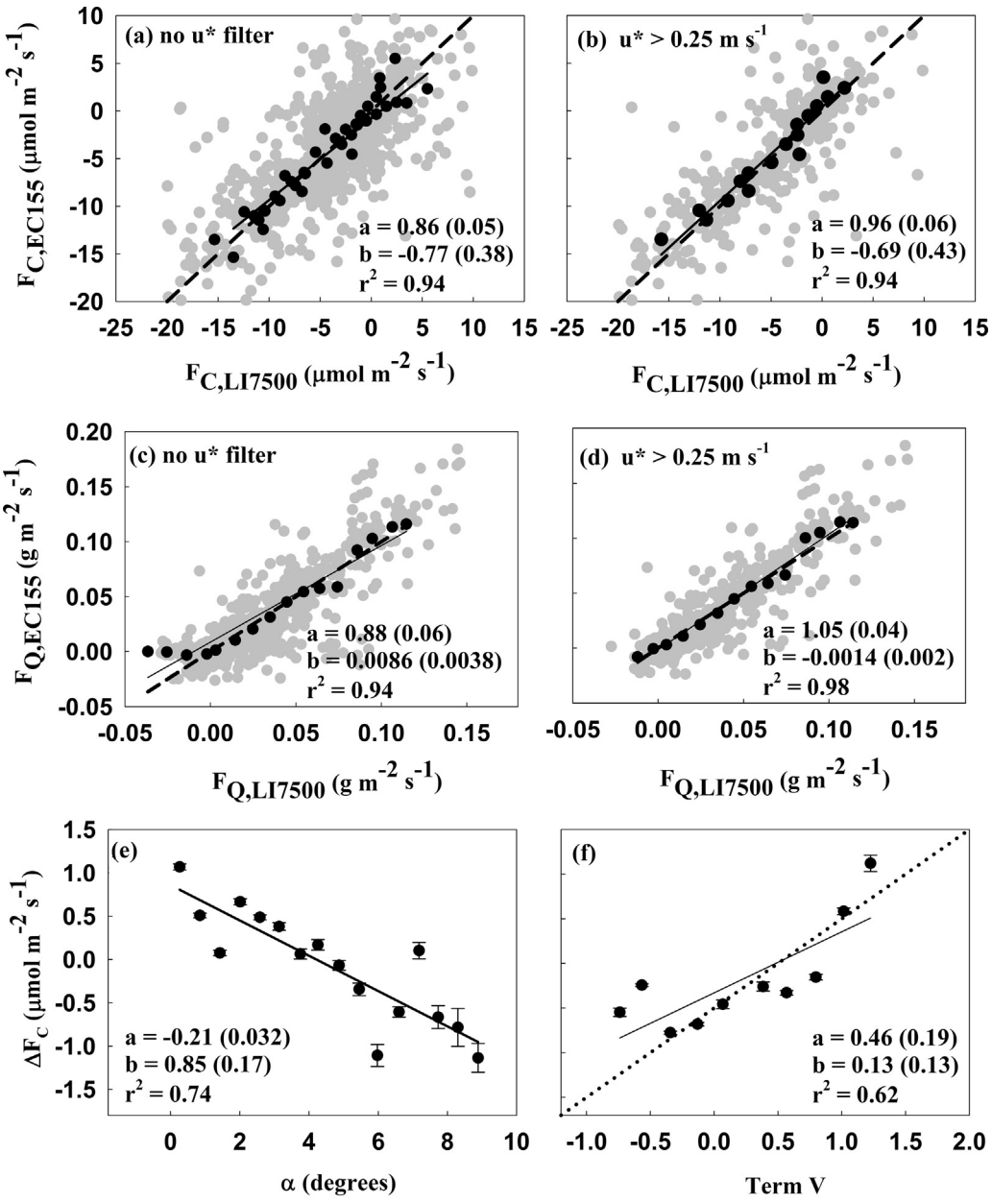

Fig. 11. The top panels show the comparison between CO_2 fluxes measured with the EC155 system and CO_2 fluxes measured with a co-located open-path (LI-7500) system deployed from 1 August 2011 to 15 December 2011. Regressions were determined from binned averages (black circles, where data were divided into bins according to the value of the independent variable in each figure) in order to permit linear regressions driven by the full range of data (as opposed to the large number of data points associated with carbon fluxes of small magnitude). All hourly data are also shown as gray circles, and data are shown before (a) and after (b) the application of a friction velocity (u^*) filter, respectively. The magnitude of the difference between the unfiltered flux records (ΔF_C) is related to the angle of attack (α, panel c), and to modeled flux correction related to self-heating of the LI-7500, (Term V, panel d). The dotted lines in panels a, b, and d show 1:1 lines for comparison. Descriptive statistics for the parameters of the regression line $y = ax + b$ are shown in each subplot, with the standard error for a and b given in parentheses.

system (Fig. 2a), and similar in shape to heat and momentum flux co-spectra (Fig. 2c,d). Some high frequency co-spectral flux attenuation was clearly evident for water vapor fluxes (Fig. 2b). This attenuation was also evident in the power spectra comparisons (Fig. 3), suggesting the decay is driven by functioning of the gas analyzers as opposed to the sonics. We further show the spectral loss was related to humidity effects (Fig. 4). However, results from an ogive analysis (Fig. 7) suggested that less than ~2% of measured water vapor fluxes were generated by eddies with timescales that correspond to frequencies of $n = 2$ or greater, which is the frequency range at which the water vapor flux loss is most apparent (Fig. 2b). Thus, while the water vapor flux attenuation is important to characterize and consider, in general these losses were small. The co-spectra for $\overline{u'w'}$ and $\overline{w'T'}$ measured by the sonics associated with the EC155 and the co-located LI-7500 were similar (Fig. 2c,d), though inspection of the power spectra for w and T suggest greater spectral power at high frequencies in the data measured by the sonic associated with the LI-7500. This disagreement may indicate the presence of tower distortion effects or tilt errors, noting that vertical velocity has been recently shown to be very sensitive to variations in the angle of attack (Kochendorfer et al., 2012; Nakai and Shimoyama, 2012), which can be large in this topographically complex site.

Finally, we note that the EC155 often performed better than the open-path LI-7500 system during early- to mid-morning periods (Fig. 13). While this tower is not equipped with an instrument

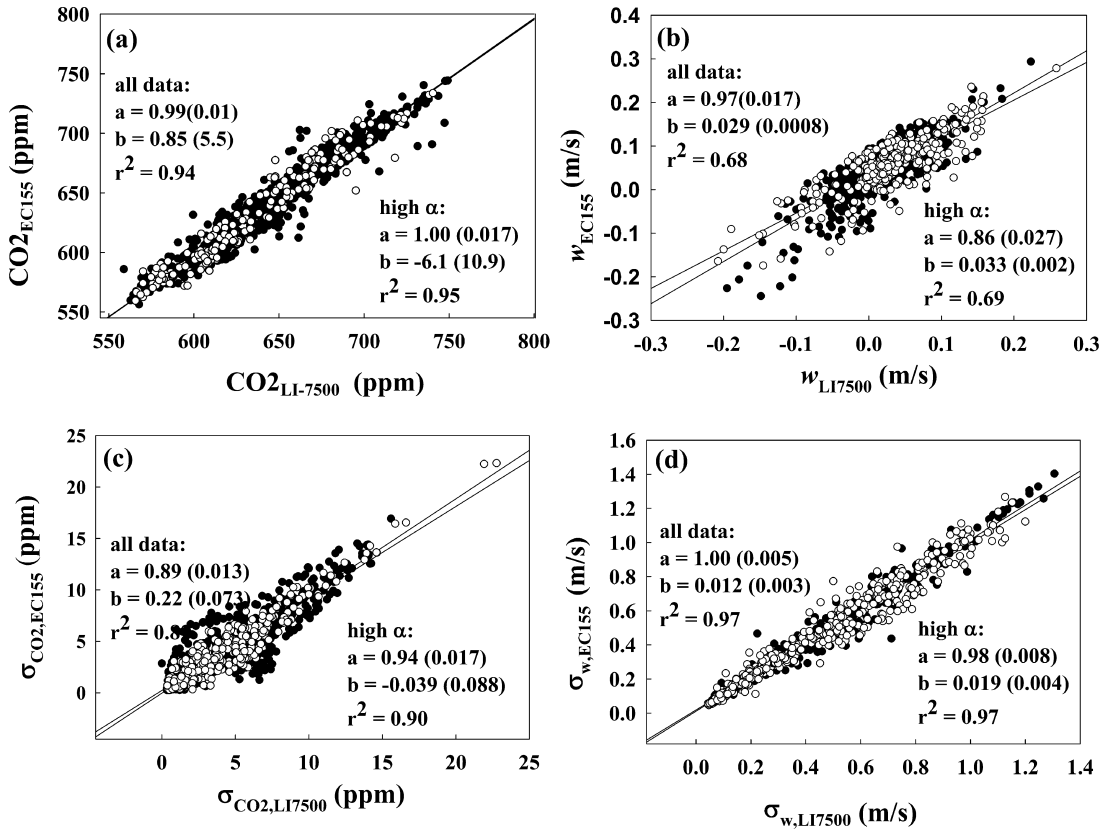

Fig. 12. Comparisons of the mean CO_2 concentration (a) measured with the EC155 as compared to the LI-7500, and vertical wind speed (w, panel b) measured with the RMYoung sonic associated with the EC155 and the CSAT3 sonic associated with the LI-7500. Cross-system comparisons of the standard deviations of these variables are shown in panels c and d. Closed symbols show data collected when the angle of attack (α) was less than 5°, and open symbols show data collected when α was greater than 5°.

specifically designed to detect the presence of fog, the anomalies in the LI-7500 measurements were generally associated with periods of high humidity (Fig. 13b), similar incident and out-going long-wave radiation (Fig. 13c), rapid increases in shortwave radiation after day break (Fig. 13d), and no precipitation, which taken together are indicators of fog events. Given the frequent occurrence of fog events in the southern Appalachian mountains in the spring and fall, these data highlight the importance of utilizing an enclosed- or closed-path analyzer for long-term flux measurements at this site.

5.2. Appropriateness of the M21 approach to correct for spectral loss

Visual inspection of the co-spectra confirm that the data may be well represented by Eq. (2) (Fig. 5), suggesting that the M21 transfer function approach is appropriate for these flux records. For a more quantitative assessment, we examined the parameters of a more general co-spectral model (i.e. Eq. (4)). During near-neutral conditions, the slope parameter m ranged from 0.74 for the open-path system momentum flux to 0.86 for the EC155 CO_2 flux (Table 4). A slope of $m = 0.75$ corresponds to a power-law decay of −7/3 in the inertial subrange, which is the classically predicted rate of decay for flat terrain (Kaimal et al., 1972; Lumley, 1967). A slope of $m = 1$ corresponds to a power law decay of −2, which is the rate of decay assumed by the M21 model. Thus, for near-neutral conditions, the co-spectra from this experiment decayed at rates that fall between the classic inertial subrange decay rate and the −2 decay rate selected by M21, which has experimental support from some recent studies (Bos et al., 2007, Cava and Katul, 2012, Su et al., 2004). The slope parameter tended to be lower during stable conditions (Table 4), with the minimum observed slope of $m = 0.65$ for the open-path CO_2 flux record. One explanation for variation in the rate of decay comes from a recent study (Cava and Katul, 2012) showing that when the co-spectral production term at z_r is not large (presumably due to a small mean scalar concentration gradient), then the co-spectral slope approaches −2. However, when the mean scalar concentration gradient is large, the −7/3 power-law prevails.

For near-neutral conditions, the maximum frequency parameter n_x was within the range of 0.14 to 0.22 for all fluxes, which is similar to the magnitude of n_x reported for open-path system flux records analyzed by Massman and Clement (2004) in a formal error analysis of the M21 approach. As expected, for all fluxes and systems, the magnitude of n_x shifted toward higher frequencies during stable conditions, reflecting less flux contribution from larger and slower moving eddies, which are more rare during stable nighttime conditions. The normalization parameter A_0 is included in Table 4 for completeness, though its magnitude is not important for the application of the M21 approach. Finally, the magnitude of the broadness parameter, u, was between 0.4 to 0.5 for most co-spectra. These spectra were thus more broad than those described by Massman and Clement (2004), which are characterized by $u \sim 0.6$, and more similar to the flat-terrain, unstable-atmosphere co-spectra of Kaimal et al. (1972), which are characterized with $u = 0.5$. In conclusion, our decision to use the M21 approach to correct our measured co-spectra were based largely on the similarity of the parameters described in Table 4 to those predicted for flat terrain co-spectral and to those described in the error analysis of Massman and Clement (2004).

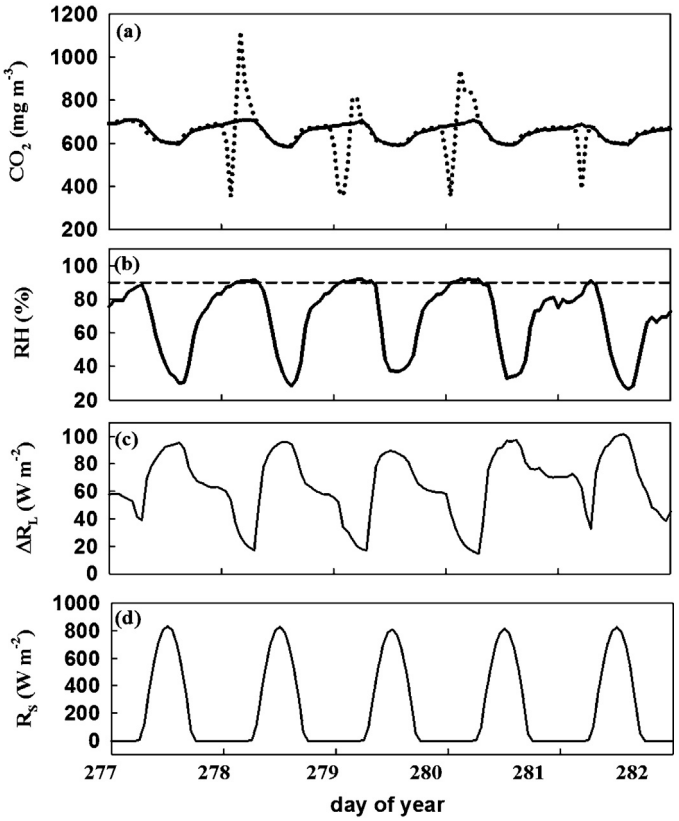

Fig. 13. Panel (a) shows the time series of CO_2 concentration measured with the EC155 (solid line) and the LI-7500 (dotted line) from DOY 277–DOY 282, 2011. Relative humidity (RH) is shown in panel (b), the difference between outgoing and incident long-wave radiation (ΔR_L) is shown in (c), and incident shortwave radiation (R_S) is shown in (d). No precipitation was recorded on these days. The horizontal dashed line in panel (b) indicates 90% RH.

5.3. Comparison to other eddy covariance systems

For a relatively short portion of the study period (30 August–5 September, 2011), the PECS was deployed on the tower at the same height as the EC155. Fluxes were measured by the PECS station using both an LI-7200 and an LI-7500 open-path system. Agreement between the EC155 and LI-7200 data records was good (Fig. 10 a,b), and better for latent heat as compared to CO_2 fluxes ($r^2 = 0.98$ and $r^2 = 0.83$, respectively).

In a previous study, better agreement between co-located LI-7200 and LI-7500 eddy covariance systems was reported ($r^2 = 0.96$, Burba et al., 2010). In the present study, the flux comparison was challenged by a divergence in wind speed measurements from the PECS and Coweeta sonic anemometers when wind direction was from the NE, which was likely caused by interference by structural elements of the tower. Consequently, many of the daytime flux data collected during the comparison period were filtered due to poor wind conditions. Thus, the comparison presented in Fig. 10a is largely driven by fluxes collected in afternoon and nighttime periods, and the inclusion of additional negative daytime carbon flux measurements would likely increase the correlation between the two datasets. The water vapor flux comparison may be less sensitive to the removal of the daytime flux measurements as the nocturnal water vapor fluxes fluxes are near zero (Fig. 10c).

Biases were also evident in the comparison between the EC155 fluxes and those measured with the LI-7500 open-path system deployed for five months of the study period (Figs. 10b,d, and 11). Attributing these sources of these biases is complicated by the fact that the EC155 system, the PECS systems, and the LI-7500 system deployed for five months are all linked to different sonic anemometers, and thus differences in measured fluxes may be attributable to differences in both sonic anemometer and gas analyzer functioning. However, we note that the PECS LI-7200 analyzers and LI-7500 analyzers were linked to the same sonic, and agreement between carbon and water vapor fluxes measured with the EC155 and the LI-7200_{PECS} system was better than agreement between carbon and water vapor fluxes measured with the EC155 fluxes and the LI-7500_{PECS} (Fig. 10). Thus, it is reasonable to assume that errors in the EC155-LI-7500_{PECS} comparison are dominated by differences in the functioning of the gas analyzers. But since the PECS system was only deployed for a short time, a better understanding of sources of error in the flux comparison is permitted by comparing fluxes measured with the EC155 and the LI-7500 system deployed for five months (i.e. Fig. 11). In particular, we explored how the difference between $F_{C,EC155}$ and $F_{C,LI7500}$ fluxes related to two variables: (1) the wind angle of attack, which can become large (5–10° or greater) at this hilly site, and (2) Term V of Eq. (8), which is related to open-path analyzer self-heating.

The magnitude of the difference between $F_{C,EC155}$ and $F_{C,LI7500}$ fluxes (i.e. $F_{C,EC155} - F_{C,LI7500}$) increased as a function of the wind angle of attack (Fig. 11e). Turbulent flux estimates are sensitive to errors in vertical wind speed, which may be related to dynamic offsets representing flow distortions around anemometer struts or the tower itself (Kochendorfer et al., 2012; Heinesch et al., 2007) and tilt-angles related to sonic orientations that are not precisely vertical with respect to gravitational potential (Lee et al., 2004). A sector-wise coordinate rotation scheme was applied before determination of EC155 and LI-7500 fluxes (but with unique rotation coefficients for each sonic); thus, flux biases related to tilt angles should be minimized, though other instrument biases and errors related to tower distortion may persist. It is possible that α may also affect the functioning of the analyzers, and in particular the LI-7500 which is sensitive to wake effects (Burba et al., 2008). Limiting data to those collected when α is high does not strongly affect the agreement between the standard deviation of CO_2 concentration, the standard deviation of w, or the mean CO_2 concentration measured with the two systems (Fig. 12a–c); however, limiting data to high α significantly affects agreement between the mean w measured with the two systems (Fig. 12d). Thus, errors in w for high α are a feasible explanation for the observed relationship between ΔF_c and α, and one which is supported by the bias reduction after u^* filtering (Fig. 11a–d), as α tends to be greatest when u^* is low. In support of this conclusion, we note that the comparison of EC155 fluxes and the PECS LI-7200 flux records relied on data that was subjected to an angle-of-attack filter according to PECS protocols, and as expected, biases in those records were small (Fig. 10a,c). Furthermore, we note that the difference in sensible heat flux between the sonic associated with the EC155 and the sonic associated with the LI-7500 is also positively correlated with α ($r^2 = 0.65$). Nonetheless, a flux comparison experiment conducted over relatively flat terrain where large α do not frequently occur would also be a valuable study informing an assessment of the functioning of the EC155.

The difference ΔF_c was also related to Term V ($r^2 = 0.50$, Fig. 11f) which is a modeled variable designed to accommodate apparent heat fluxes caused by self-heating of the LI-7500. This relationship reflects biases related to analyzer functioning, though the magnitude of ΔF_c was typically lower than predicted by Term V. This discrepancy could suggest that the empirical relationships linking instrument temperature to meteorological variables presented by Burba et al. (2008) are not universal. It could also point to a bias between the systems that is not related to instrument heating. In any event, the relationship between ΔF_c and Term V also disappears after u^* filtering, which is not surprising as instrument heating tends to be highest when air temperatures and wind speed are low (periods that tend to be characterized by low u^*). Thus, to

summarize, the observed biases in carbon and water fluxes measured with the EC155 and the open-path systems are likely related to errors in both sonic functioning and analyzer functioning, all of which are minimized after the application of a friction velocity filter.

5.4. The use of the mixing ratio approach for flux calculation

Consistent with other recent studies (Burba et al., 2012; Nakai et al., 2011) relying on data from LI-7200 analyzers, we show that EC155 fluxes calculated from the instantaneous mixing ratio agreed well with EC155 WPL-corrected mass–density flux measurements (Fig. 9a). Thus, with this new class of enclosed-path analyzers, it is possible to avoid WPL density corrections entirely in post-processing of the data. However, given the very high correlation between mixing ratio and mass–density based fluxes measured with enclosed closed-path systems (after WPL terms have been applied) reported here and in other studies, the advantage of using the mixing ratio approach is realized primarily as a reduction in the number of steps involved in the flux processing.

6. Conclusion

With the recent advent of fast-response, enclosed path analyzers, members of the growing eddy covariance research community have more options to consider when designing a new flux monitoring site. These new analyzers may also prove useful in identifying biases in flux records on an individual site or across broader flux networks. Here, we confirmed that co-spectra for CO_2 flux measured with the EC155 are similar to those measured with a co-located open-path system, and that the shape of the co-spectra permit the application of the M21 analytical spectral correction approach. We also showed that EC155 fluxes calculated with the mixing ratio approach agree well with fluxes calculated from EC155 mass–density measurements, confirming and extending the results of similar studies (Burba et al., 2012; Nakai et al., 2011) conducted with LI-7200 analyzers. When these results are taken together, they suggest that high frequency variations in the gas mixing ratios are accurately measured by the EC155; nonetheless, an independent experiment to confirm the field accuracy of the EC155 pressure and temperature cell would be a valuable compliment to this study. Finally, we demonstrate that the EC155 system significantly outperforms co-located open-path analyzers during adverse weather conditions such as fog events, which occur frequently in the southern Appalachians. Thus, the EC155 appears to be a good instrument choice for the new Coweeta eddy covariance tower. We note that the proximity of the tower to the Coweeta headquarters (<1 km) permitted ready access to the analyzer for routine calibration and maintenance. However, these instruments may also be suitable for more remote deployments as the systems may be configured for automated zero/span checks and remote calibrations which are not possible with open-path systems.

Acknowledgments

Support for this work was provided by the U.S. Department of Energy (Grant no. DE-FG02-06ER6430). This document has been reviewed in accordance with U.S. Environmental Protection Agency policy and approved for publication. Mention of trade names or commercial products does not constitute endorsement or recommendation for use. We thank a number of individuals who assisted with data collection and analysis, including Steven Brantley, Chelcy Ford, Randy Fowler, Stephanie Laseter, and Andres Schmidt. We are grateful to Gaby Katul, William Massman, and Chelcy Ford for providing valuable comments on a previous version of this manuscript.

References

Aubinet, M., Feigenwinter, C., Heinesch, B., Bernhofer, C., Canepa, E., Lindroth, A., Montagnani, L., Rebmann, C., Sedlak, P., Van Gorsel, E., 2010. Direct advection measurements do not help to solve the night-time CO_2 closure problem: evidence from three different forests. Agric. For. Meteorol. 150, 655–664.

Bos, W.J.T., Shao, L., Bertoglio, J.-P., 2007. Spectral imbalance and the normalized dissipation rate of turbulence. Phys. Fluids 045101, http://dx.doi.org/10.1063/1.2714079

Burba, G.G., McDermitt, D.K., Grelle, A., Anderson, D.J., Xu, L.K., 2008. Addressing the influence of instrument surface heat exchange on the measurements of CO_2 flux from open-path gas analyzers. Global Change Biol. 14, 1854–1876.

Burba, G.G., McDermitt, D.K., Anderson, D.J., Furtaw, M.D., Eckles, R.D., 2011. Novel design of an enclosed CO_2/H_2O gas analyser for eddy covariance flux measurements. Tellus Ser. B 62, 743–748.

Burba, G., Schmidt, A., Scott, R.L., Nakai, T., Kathilankal, J., Fratini, G., Hanson, C., Law, B., McDermitt, D.K., Eckles, R., Furtaw, M., Velgersdyk, M., 2012. Calculating CO_2 and H_2O eddy covariance fluxes from an enclosed gas analyzer using an instantaneous mixing ratio. Global Change Biol. 18, 385–399.

Cava, D., Katul, G.G., 2012. On the scaling laws of the velocity-scalar cospectra in the canopy sublayer above tall forests. Bound.-Layer Meteorol., http://dx.doi.org/10.1007/s10546-012-9737-2

Detto, M., Katul, G.G., 2007. Simplified expressions for adjusting higher-order turbulent statistics obtained from open-path gas analyzers. Boundary Layer Meteorol. 122, 205–216.

Feigenwinter, C., Bernhofer, C., Vogt, R., 2004. The influence of advection on the short term CO_2 budget in and above a forest canopy. Boundary Layer Meteorol. 113, 201–224.

Foken, T., Göckede, M., Mauder, M., Mahrt, L., Amiro, B.D., Munger, J.W., 2004. Post-field data quality control. In: Lee, X. (Ed.), Handbook of Micrometeorology: A Guide for Surface Flux Measurements. Kluwer Academic Publishers, Dordrecht, pp. 81–108.

Goulden, M.L., Daube, B.C., Fan, S.-M., Sutton, D.J., Bazzaz, A., Munger, J.W., Wofsy, S.C., 1997. Physiological responses of a black spruce forest to weather. J. Geophys. Res. Atmos. 102, 28987–28996.

Haslwanter, A., Hammerle, A., Wohlfahrt, G., 2009. Open-path vs. closed-path eddy covariance measurements of the net ecosystem carbon dioxide and water vapour exchange: a long-term perspective. Agric. For. Meteorol. 149, 291–302.

Heinesch, B., Yernaux, M., Aubinet, M., 2007. Some methodological questions concerning advections measurements: a case study. Boundary Layer Meteorol. 122, 457–478.

Hollinger, D.Y., Goltz, S.M., Davidson, E.A., Lee, J.T., Tu, K., Valentine, H.T., 1999. Seasonal patterns and environmental control of carbon dioxide and water vapour exchange in an ecotonal boreal forest. Global Change Biol. 5, 891–902.

Ibrom, A., Dellwik, E., Flyvbjerg, H., Jensen, N.O., Pilegaard, K., 2007. Strong low-pass filtering effects on water vapour flux measurements with closed-path eddy correlation systems. Agric. For. Meteorol. 147, 140–156.

Kaimal, J.C., Wungaard, J.C., Izumi, Y., Coté, O.R., 1972. Spectral characteristics of surface-layer turbulence. Q. J. R. Meteorolog. Soc. 98, 563–589.

Kochendorfer, J., Meyers, T.P., Frank, J., Massman, W.J., Heuer, M.W., 2012. How well can we measure the vertical wind speed? Implications for fluxes of energy and mass. Bound.-Layer Meteorol. http://dx.doi.org/10.1007/s10546-012-9837-1

Lee, X.H., Finnigan, J., Paw U, K.T., 2004. Coordinate systems and flux bias error. In: Lee, X., Massman, W.J., Law, B. (Eds.), Handbook of Micrometeorology: A Guide for Surface Flux Measurement and Analysis. Kluwer Academic, Dordrecht/Boston/London.

Lee, X.H., Massman, W.J., 2011. A perspective on thirty years of the Webb, Pearman and Leuning density corrections. Boundary Layer Meteorol. 139, 37–59.

Leuning, R., Judd, M.J., 1996. The relative merits of open- and closed-path analysers for measurement of eddy fluxes. Global Change Biol. 2, 241–253.

Leuning, R., 2004. Measurements of trace gas fluxes in the atmosphere using eddy covariance: WPL corrections revisited. In: Lee, X., Massman, W.J., Law, B. (Eds.), Handbook of Micrometeorology: A Guide for Surface Flux Measurement and Analysis. Kluwer Academic, Dordrecht/Boston/London.

Leuning, R., 2007. The correct form of the Webb, Pearman and Leuning equation for eddy fluxes of trace gases in steady and non-steady state, horizontally homogeneous flows. Boundary Layer Meteorol. 123, 263–267.

Lumley, J.L., 1967. Similarity and the turbulent energy spectrum. Phys. Fluids 10, 855–858.

Mammarella, I., Launiainen, S., Gronholm, T., Keronen, P., 2012. Relative humidity effect on the high-frequency attenuation of water vapor flux measured by a closed-path eddy covariance system. J. Atmos. Oceanic Technol. 26, 1856–1866.

Massman, W.J., 2000. A simple method for estimating frequency response corrections for eddy covariance systems. Agric. For. Meteorol. 104, 185–198.

Massman, W.J., 2001. Reply to comment by Rannik on a simple method for estimating frequency response corrections for eddy covariance systems. Agric. For. Meteorol. 107, 247–251.

Massman, W.J., Lee, X., 2002. Eddy covariance flux corrections and uncertainties in long-term studies of carbon and energy exchanges. Agric. For. Meteorol 113, 121–144.

Massman, W.J., Clement, R., 2004. Uncertainty in eddy covariance flux estimates resulting from spectral attenuation. In: Lee, X., Massman, W.J., Law, B. (Eds.), Handbook of Micrometeorology: A Guide for Surface Flux Measurement and Analysis. Kluwer Academic Publishers, Dordrecht/Boston/London.

Massman, Ibrom, W.J.A., 2008. Attenuation of concentration fluctuations of water vapor and other trace gases in turbulent tube flow. Atmos. Chem. Phys. 8, 9819–9853.

Nakai, T., Iwata, H., Harazono, Y., 2011. Importance of mixing ratio for a long-term CO_2 flux measurement with a closed-path system. Tellus Ser. B 63, 302–308.

Nakai, T., Shimoyama, K., 2012. Ultrasonic anemometer angle of attack errors under turbulent conditions. Agric. For. Meteorol. 162, 14–26.

Paw U, K.T., Baldocchi, D.D., Meyers, T.P., Wilson, K.B., 2000. Correction of eddy-covariance measurements incorporating both advective effects and density fluxes. Boundary Layer Meteorol. 97, 487–511.

Rannik, U., Vesala, T., Keskinen, R., 1997. On the damping of temperature fluctuations in a circular tube relevant to the eddy covariance technique. J. Geophys. Res. 102, 12789–12794.

Reverter, B.R., Carrara, A., Fernandez, A., Gimeno, C., Sanz, M.J., Serrano-Ortiz, P., Sanchez-Canete, E.P., Were, A., Domingo, F., Resco, V., Burba, G.G., Kowalski, A.S., 2011. Adjustment of annual NEE and ET for the open-path IRGA self-heating correction: magnitude and approximation over a range of climate. Agric. For. Meteorol. 151, 1856–1861.

Schmid, H.P., Grimmond, C.S.B., Cropley, F., Offerle, B., Su, H.B., 2000. Measurements of CO_2 and energy fluxes over a mixed hardwood forest in the mid-western United States. Agric. For. Meteorol. 103, 357–374.

Schmidt, A., Hanson, C., Chan, W.S., Law, B.E., 2012. Empirical assessment of uncertainties of meteorological parameters and turbulend fluxes in the Ameriflux networl. J. Geoophys. Res. 11, 7, http://dx.doi.org/10.1029/2012JG002100.

Siqueira, M.B., Katul, G.G., 2010. An analytical model for the distribution of CO_2 sources and sinks, fluxes, and mean concentration within the roughness sub-layer. Boundary Layer Meteorol. 135, 31–50.

Su, H.B., Schmid, H.P., Grimmond, C.S.B., Vogel, C.S., Oliphant, A.J., 2004. Spectral characteristics and correction of long-term eddy-covariance measurements over two mixed hardwood forests in non-flat terrain. Boundary Layer Meteorol. 110, 213–253.

Webb, E.K., Pearman, G.I., Leuning, R., 1980. Correction of flux measurements for density effects due to heat and water-vapor transfer. Q. J. R. Meteorol. Soc. 106, 85–100.

Wilczak, J.M., Oncley, S.P., Stage, S.A., 2001. Sonic anemometer tilt correction algorithms. Boundary Layer Meteorol. 99, 127–150.